



Investigation of Air Flow Characteristics in Air Intake Hoses using CFD and Experimental Analysis based on Deformation of Rubber Hose Geometry

K. Furkan Sokmen[†] and O. Bedrettin Karatas

Bursa Technical University, Faculty of Engineering and Natural Science, Mechanical Engineering Department, Bursa, 16330, Turkey

[†]Corresponding Author Email: furkan.sokmen@btu.edu.tr

(Received May 8, 2019; accepted October 12, 2019)

ABSTRACT

In this study, the pressure loss value of air intake hose of FIAT 1.3 E6D type engine, located between intercooler and inlet manifold of the engine, was examined using computational fluid dynamics, considering geometrical deformation in a rubber material. The rubber material modelling was performed by the verification of the data - obtained through the experimental method- with ANSYS software using Mooney-Rivlin method. The rubber material modelling was performed with the aim of correctly determination of the increase in the hose diameter when subjected to pressure, since the material has the feature of elasticity. In this study, ANSYS Fluent v.18.0 software and a static pressure machine were used. The air intake into the hose took place at the pressure of 123,5 kPa and flow rate of 0,087 kg/s. A solution, independent of the number of element, was obtained in the analysis. The turbulence model used in the study is standard k- ϵ type. As a result, the deformation-oriented pressure loss in the last geometry was found 1,85 kPa. The analyses were repeated for non-deformed geometry, and a pressure loss of 2,04 kPa was determined. At the result of the test, the geometry was seen to become actually deformed, and the pressure loss was found 1,9 kPa. The lowness of pressure loss in the deformed geometry was seen as the removal of the sharp bends that would cause local losses with the effect of pressure forces. In this study, it was determined that geometrical deformation changes the geometrical features that causes pressure loss, and leads to less pressure loss.

Keywords: Air intake hose; Pressure drop; Rubber material model; Deformation; Computational fluid dynamics.

NOMENCLATURE

| | | | |
|------------------|--|------------------|---|
| Gr | Grashof number | T _{out} | air temperature at the outlet of the hose |
| h | heat convection coefficient | ΔT | value of change in temperature |
| Nu | Nusselt number | ΔP_K | total pressure loss |
| P _{in} | inlet pressure value | ϵ_{PA} | surface roughness coefficient of PA6GF15 |
| Re _{in} | Reynold number at the inlet of the hose | ϵ_{CR} | surface roughness coefficient of rubber |
| T _{in} | air temperature at the inlet of the hose | | |

1. INTRODUCTION

The main function of the air hose is to provide to intake sufficient amount of air into engine, with enough purity. The air hose has three main functions. The first one is to provide to intake sufficient amount of air, required for an efficient combustion, the second one is to provide the purity of air, and the third one is to provide for engine to operate under the specified sound level. It has been reported in relevant

studies that the failure in taking air at required pressure cause fuel consumption to increase (Abdullah *et al.* 2013; Mamat, Rosli Abdullah, Xu, Wyszynski, & Tsolakis, 2017). It has also been reported that even a minor impermeability problem would cause serious efficiency losses in the engine. That's why, it should be noted in the air hose design that the material to be selected and its geometric design should be durable against exterior factors (Baaser 2007). Computational Fluid Dynamics

(CFD) applications have brought great cost and prediction advantages in the fields, such as aerodynamic inspections and air hose systems at automotive industry, where significant calculations are required to be made (Ramasamy *et al.* 2010). Besides, finite element method has been widely used in automotive industry, providing it to get rid of high test costs and test investments (Gu 2017).

William *et al.* studied on the intake manifold design of a 600cc formula vehicle. In their study, they aimed to minimize geometric design restriction- dependent pressure losses (Williams and Ilardo 2010). Ramasamy *et al.* examined a winglet- added air intake system by CFD, which reduces pressure losses on air filter and auxiliary for air filter. In their study they used standard k- ϵ turbulence model. In the result of the study, pressure losses, with the addition of a wing let and without winglet, were determined at different engine velocities (Ramasamy *et al.* 2010). Gobel performed CFD analyses of a sample air intake system. In this study, pressure losses, at different engine velocities, filter application- dependent, were determined. Standard High Reynolds number k- ϵ turbulence model was used in the CFD analysis. Interconsistent results were obtained at the result of test and analyses (Gohel 2015). In addition, Yerram *et al.* made a study on the analysis of air intake system using CFD system. In this study, an optimization study was carried out on a geometry, different from that used in other studies, and progresses in the flow were followed (Yerram and Prasad 2018). Sedlacek and Skovajsa (2016) conducted a study on the CFD analyses of air intake systems and geometric optimization. It was done on an one- dimensional model (Sedlacek and Skovajsa 2016). In their study, Safwan and Lothfy made the analyses of the pressure losses of Proton Waja 1.6 trade mark vehicle, at various engine cycles using CFD system, and defined the critical locations in the system. High Reynolds number k- ϵ turbulence model was used in the analyses (Safwan and Lothfy, 2009). Choi and Oh (2010) examined the change of shape of fibrous structure- included in air hose material- in radial direction at high temperature and pressure both using FEM method and tests. (Choi and Oh 2010), Kamarulbaharin and Kasolang (2015), in their study, examined the dynamic pressure distribution in air hose. As a result of their studies, they found that the pressure values were approximate throughout the air hose, at various engine velocities (Kamarulbaharin and Kasolang 2015).

Chaubey and Tiwari (2017) made a study on the intake manifold of Suzuki G13bb engine. ANSYS commercial software was used in the study. In the study, it was aimed to supply required air flow into the engine, with minimum pressure loss. In the study made using CFD system, the most suitable turbulence model was sought, and found that standard k- ϵ turbulence model was suitable (Chaubey and Tiwari 2017).

An exemplary image is shown for an air intake system in Fig. 1.

In a similar study, Bhakade and Patil analysed the geometric deformation on rubber hose using CFD

and FEA methods. They used realizable k- ϵ turbulence model in the CFD analysis. They used Marlow model for FEM method. As a result of the study, maximum deformation determined was 0,401. But , in the study, whether this deformation had any effect on pressure loss wasn't examined (Bhakade *et al.* 2016).

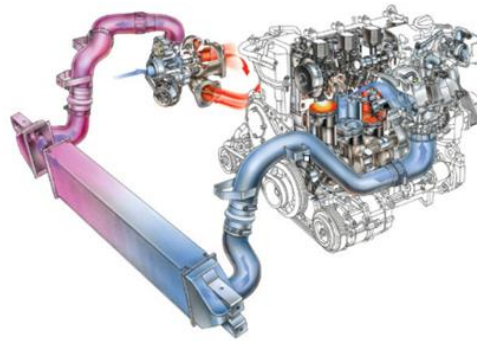


Fig. 1. An air intake system.

Another study was conducted by Kumar and Genasan. In the study, pressure loss analyses of the air hose and their verification by tests were investigated. The experimental measurements and analyses were found interconsistent in the study done using fluent software. The turbulence model used in the study is standard k- ϵ model. The convergence criterion applied is 10^{-3} (Kumar and Ganesan 2004).

Uysal *et al.* examined thermal and momentum characteristics of intercooler connection hose with CFD analysis. In the study, the effects of vibration on pressure loss were tested. During the study, the analyses of vibration at high temperature were performed with fluid-structure interaction (FSI) method. It was seen that vibration increases pressure loss (Uysal *et al.* 2012).

Liquid-solid interaction solutions have get started to gain great importance in engineering applications. In the study by Rao (2003), the pressure distribution- dependent geometric deformation was determined with FSI method, in ANSYS software (Rao 2003).

Kumar and Rao used Mooney Rivlin model in order to model the mechanical behaviors of hyperelastic materials, and they verified the results through experimental data (Kumar and Rao 2016).

In this study, the total pressure loss of air hose used at FIAT 1.3 E6D (Fig. 2) engine was performed with numerical and experimental methods. The analyses and tests were carried out in accordance with Subsystem Functional Description for Charge Air Hoses Fiat 225 Euro 5" FIAT standard. Different from other studies, the geometric change at rubber hose, occurring with the effect of compressive forces, was examined in this study. Unlike the other studies, the effect of the geometric deformation on total pressure loss at the rubber hose part of air hoses was focused on in the study done in real working conditions. FSI method used in the study by Uysal *et al.* (2012) was used in order to determine the

behavior of air hose in real working conditions, and Mooney-Rivlin method used in the study by Kumar ve Rao was used in order to create rubber material model. The material tests were performed to establish rubber material model correctly, and error ratio was decreased in determining geometric deformation.



Fig. 2. FIAT 1.3 E6D Air intake hose.

2. MATERIAL AND METHODS

2.1 Geometry Model

The air intake hose located between the intercooler and intake manifold consisted of various components. At the intercooler side, Para-Aramid-reinforced CR (Chloroprene Rubber), which is suitable for working under high pressure, temperature and vibration, was recommended in the OEM's standards. At the intake manifold side, Polyamide 6 GF 15, which is suitable for same working conditions, was preferred. There were some connection components on the hose: a Henn HC 45 quick connector which provides easy assembly to the intercooler output spigot during the manufacturing process of the vehicle, located at the end of the CR rubber hose. CR rubber hose was connected to a PA 6 GF 15 (chemically strengthened with 15% glass fiber pipe) by a Visa E clamp. The polyamide pipe was assembled to the vehicle body with a PA6 GF15 bracket located at the bottom side of the pipe and near the rubber hose in order to provide dimensional stability and prevent deformation of the pipe under engine vibration. It is welded onto the pipe. The role of the brackets made from PA6 GF15 was connection of the clips. The PA6 GF15 flange was connected to end of the plastic pipe and welded on the pipe. It contained two AISI304 spacers for assembly to the engine manifold with screws (Fig. 3).

The length, diameter and thickness of the hose were respectively 689 mm, 40 mm and 4 mm.

2.2 Experiment for Material Selection

Expansion of the diameter is observed due to the hose's elastic structure when the pressure passes through it. This expansion depends on the intensity of pressure and the mechanical properties of the material. Since PA6 GF 15 is a standard plastic material, its mechanical properties are also including in the ANSYS material database. However, CR, which was used in the rubber part of the hose, was produced in the dough department by making improvements to meet the Fiat specifications. For this reason, there was no material in the ANSYS

material database that would meet its mechanical properties one to one. The analysis should be carried out according to the worst conditions (enlarged diameter) so that diameter expansion will increase the pressure loss. In order to calculate the mechanical behavior of the reinforced rubber hose, a tension test was performed on several specimens in the laboratory. To obtain orthotropic properties, longitudinal and lateral specimens were tested (Fig. 4).

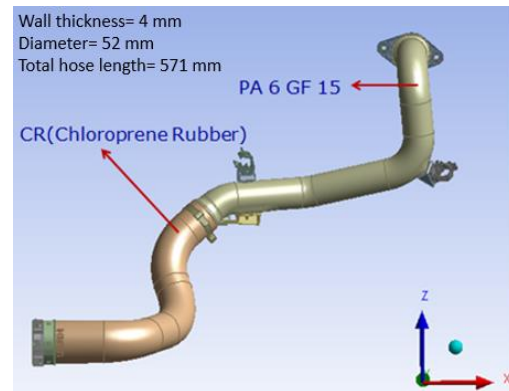


Fig. 3. Air intake hose geometry.

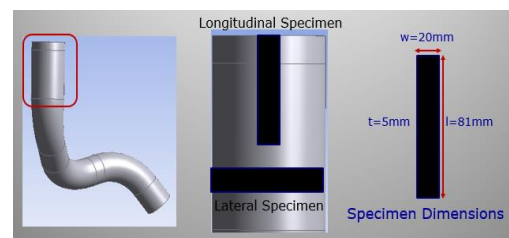


Fig. 4. Specimens for tension test.

A force-deflection plot was obtained by tensile tests on longitudinal and lateral samples (Fig. 5). There were strain values of up to 50% (40 mm deflection), and the force-deflection values were very close to each other in longitudinal and lateral direction specimens. Furthermore, under an internal pressure loading of 123.5 kPa, the strain value on the reinforced rubber did not exceed 50% strain. For this reason, it was concluded that there was no need to use the orthotropic material model. One of the Force-Deflection Curves that were obtained is given as an example.

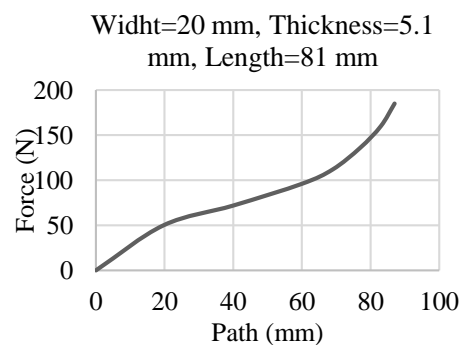


Fig. 5. Force-deflection curve for a specimen.

To obtain the mechanical properties of the rubber material, the Mooney-Rivlin Material Model was used. Rubber is a “Hyper elastic material” which has large elastic strains and deformations. It shows nonlinearity as in Fig. 6 and large deformation (Kumar and Rao 2016). The stress state in the hyper plastic material was determined by taking the derivatives of the strain energy density with respect to the strain components. A suitable model was used based on the type of the stress-strain curve.

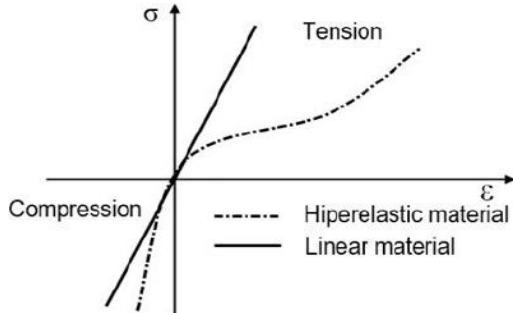


Fig. 6. Stress-Strain curves for hyper elastic and linear materials.

The strain energy function of the Mooney-Rivlin hyper elastic model is defined as a function of strain invariants $I_1, I_2, I_3 = f_2$. Strain energy density function of the 3-parameter model was described as shown in Table 1.

Table 1 Hyper elastic material constants

| Mooney-Rivlin 3 Parameters | |
|----------------------------|-------------|
| Material Constant C10 | -1.7882 MPa |
| Material Constant C01 | 2.5703 MPa |
| Material Constant C11 | 0.51727 MPa |

When the force-deflection curves were drawn in the same plot, it was clearly seen that the values obtained from the tension test and tension analysis fit each other very well as seen in Fig. 7. Therefore, the reinforced rubber material constants were correct.

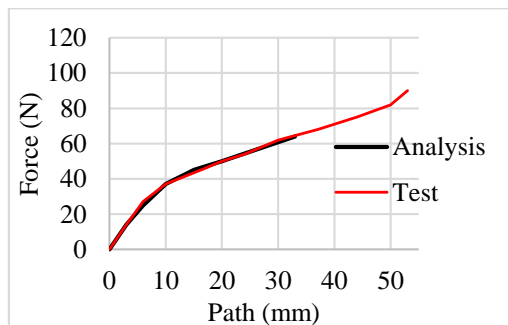


Fig. 7. Force-deflection curves created by Tension Test and ANSYS Software.

A material database created by tensile tests was defined for geometry in order to determine the material model.

2.3 Experimental Method for Performance Test

The FIAT 1.3 E6D air intake hose was subjected to

pressure tests under the required boundary conditions (123.5 kPa of air pressure) for the purpose of verifying the results of the numerical analysis. A pressure test bench located in laboratory was used for this study (Fig. 8). The properties of static pressure test cabinet is given in Table 2.



Fig. 8. Pressure test bench.

Table 2 Test cabinet properties

| | Pressure (Bar) | Temperature (°C) |
|----------|----------------|------------------|
| Range | 0-40 | 0-150 |
| Accuracy | +/- 0,01 | +/- 0,1 |

Before the test, the intercooler outlet and intake manifold inlet spigots of the FIAT 1.3 E6D engine system were manufactured on a one-to-one scale, and they were connected to the air intake hose. The air intake hose that were connected to the inlet and outlet spigots was connected to the test bench (Fig. 9).



Fig. 9. Intake hose and cabined connections.

A 1000 kPa per minute pressure increasing rate and a 123.5 kPa holding pressure were set in the software of the test bench. Dry air (100 °C) was used for the pressure drop test, and the pressure drop value was measured after a pressure stabilization time of 60 s. The ambient conditions were 1 atm and 23°C. The pressure drop value was measured as 2 kPa by the pressure transmitter.

In the FSI analysis, each time step in the solution phase is divided into a series of stagger iterations with a partitioned approach. In first step, to satisfy all types of convergence criteria in fluid-structural field equations, within each individual stagger iteration step, stagger iterations are realized. In second step, the load vectors are appraised. In the last two step,

the displacement load vectors are transferred from ANSYS to the FLUENT solvent, the fluid problem is solved and the structural problem is solved by transferring force load vectors from the FLUENT solvent to the ANSYS solvent.

2.4 Computational Study

In this study, the Ansys Fluent v.18.0 software was used to determine the pressure loss inside the hose. Mass, momentum and energy conservation equations were primarily solved in the analysis. As temperature changes the viscosity of fluids, changes in the temperature were also taken into consideration in the flow analysis.

The Reynolds number at the inlet of the hose was calculated to be $Re_{in} \approx 97 \times 10^3$. According to this value, the flow in the analysis was turbulent. The heat convection coefficient around the hose (h) was calculated using the relationships in the study conducted by Uysal *et al.* that provided the Nu and Gr numbers which were found to be 12,63 and 835433, respectively (Uysal *et al.* 2012). According to these values, the heat convection coefficient was calculated to be $h = 6.86 \text{ W/m}^2\text{K}$ and used in the analysis.

Simplification operations were applied to the geometry to be analyzed. The brackets used to fasten the hose were removed from the geometry, and only the flow area was included in the analysis.

In the analysis, the undeformed air hose was initially analyzed, and the pressure loss value was determined (Fig. 10 a). The boundary conditions were given to in Table 3. The convergence criterion was assumed 10^{-3} similar to the study Kumar and Genasan (2004). Boundary conditions were given in Table 3.

Table 3 Boundary Conditions

| Flow type | k-ε turbulence model |
|--|----------------------|
| Fluid temperature | 100°C |
| Inlet pressure (P_{in}) | 123.5 kPa |
| Mass Flow Rate (\dot{m}) | 0.087 kg/s |
| Surface Roughness for PA6 GF30 (ϵ_{PA}) | 1.85 μm |
| Surface Roughness for Rubber (ϵ_{CR}) | 0.32 μm |

Velocity and pressure was coupled by using SIMPLEC algorithm. Standard k-ε model with standard wall function was chosen by considering its robust structure and widespread using in literature. In spite of the fact that standard k-ε model has some disadvantages at separated flows, it was also preferred in this study because of having a robust structure, and of being used widely, as seen in the introduction section. The pressure distribution obtained as a result of the analysis is given in Fig. 10 b. The pressure values were included in the structural analysis, in order to define geometric deformation value. The analyses were made according to the material model specified. As a result of the FSI analyses, the deformation values that pressure forces in the hose caused on rubber hose were determined (Fig. 11 a).

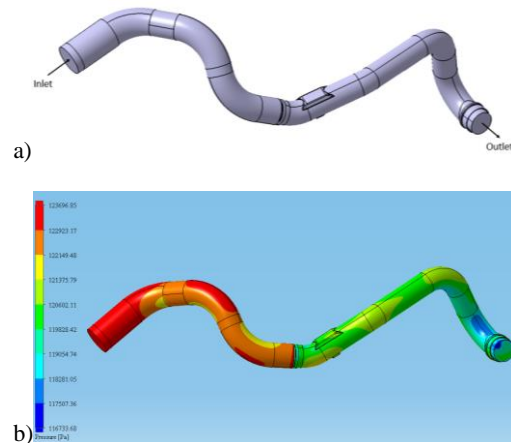


Fig. 10. a) Undeformed rubber b) Pressure distribution of hose with undeformed rubber part.

A maximum deformation of 0.29 mm was obtained in a local region on the rubber hose. The final geometry obtained with the deformation is given in Fig. 11 b. Deformation was determined during the test as well, at the region where geometric deformation was determined as maximum in the analysis.

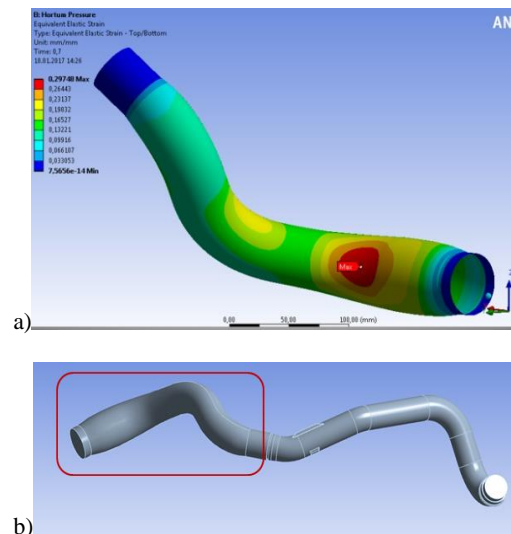


Fig. 11. a) Deformation distribution on rubber part b) All hose with deformed rubber.

The measurements taken from the diameter where maximum deformation occurred, at the end of the test, and analysis results are given in Table 4.

Table 4 Results of deformation for rubber hose

| Results | Test | Analysis | Error |
|---------|------|----------|-------|
| mm | 0.31 | 0.29 | 0.2 |

It was determined that test and analysis results were approximate, and there was a difference of 0.2 mm between them. The analysis results were obtained as independent from element number. The element structure was selected as triangular, and the element structure on the inner surface of the hose was tightened in to more precisely calculate the effects of the viscous forces (Fig. 12 a, b).

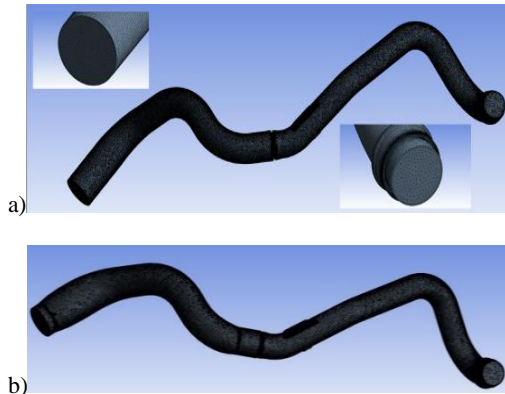


Fig. 12. a) Undeformed rubber b) Pressure distribution of hose with undeformed rubber part.

By comparison of the analysis and test results, a solution independent of the number of elements was obtained. It was determined that the values obtained for numbers of elements of 1560000 and above did not change (Table 5). After this step, both the test results were verified and the results of the analysis were not changed.

Table 5 Mesh Independency

| Element | Pressure Drop (kPa) CFD |
|---------|-------------------------|
| 780000 | 1.81 |
| 1100000 | 1.83 |
| 1560000 | 1.842 |
| 1850000 | 1.848 |
| Test | 1.9 |

The analyses were carried out at the workstation computer with 12 nucleus, having 96 GB RAM power. The analyses converged after 278 iterations. The convergence graphics of the outlet total pressure of the hose, and of minimum, maximum and average pressure values throughout the hose are given in Fig. 13 and Fig. 14.

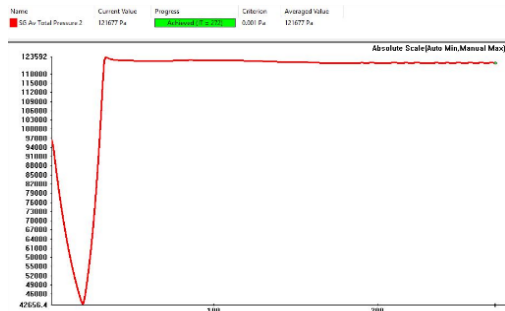


Fig. 13. Convergence screen after 278 iteration, outlet pressure.

3. RESULTS

The results obtained from the analyses made for deformed and undeformed geometries are given in Fig. 15 and Table 4, comparatively with the test results.

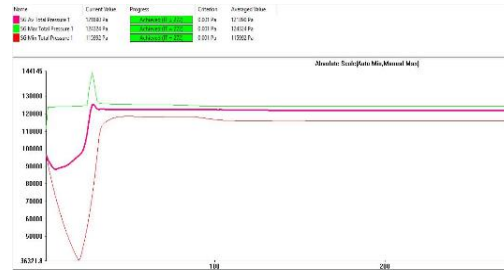


Fig. 14. Convergence screen after 278 iteration, Minimum, maximum and average pressure.

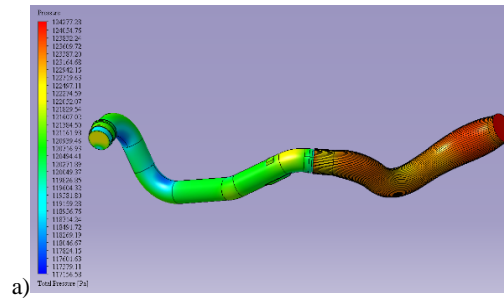


Fig. 15. Pressure distribution a) Deformed hose b) Undeformed hose.

While outlet pressure was defined as 121.677 kPa at deformed hose geometry, total pressure loss was calculated as 1.85 kPa. While outlet pressure was defined as 121.420 kPa at undeformed hose geometry, total pressure loss was calculated as 2.04 kPa (Table 6).

Table 6 CFD and Test Results

| Undeformed hose | Deformed hose | Test |
|-----------------|---------------|---------|
| 2.04 kPa | 1.85 kPa | 1.9 kPa |

7 bends that cause pressure losses on air hose are given in Fig. 16. The pressure loss values at these bends are given in Table 7 comparatively for deformed and undeformed geometry.

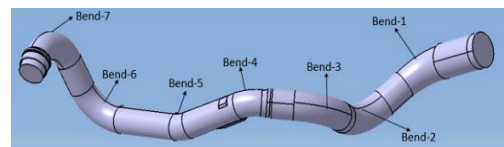


Fig. 16. Bends on air intake hose.

According to the values obtained from Table 7, Fig. 15 a and b, the total pressure loss in deformed geometry is less than that in undeformed geometry.

Table 7 Inlet and outlet pressures at the bends, pressure decreases at the bends and pressure decrease differences

| | | 123.5 kPa | ΔP_{k1} (kPa) | 123.5 kPa | ΔP_{k2} (kPa) | Dif |
|---|-----|---------------|--------------------------|---------------|--------------------------|-------|
| 1 | In. | 123.49 | 0.32 | 123.49 | 0.34 | -0.02 |
| | Ex | 123.17 | | 123.15 | | |
| 2 | In | 123.17 | 0.28 | 123.15 | 0.21 | 0.07 |
| | Ex | 122.89 | | 122.94 | | |
| 3 | Inl | 122.89 | 0.29 | 122.94 | 0.23 | 0.06 |
| | Ex | 122.60 | | 122.71 | | |
| 4 | In | 122.60 | 0.31 | 122.71 | 0.26 | 0.05 |
| | Ex | 122.29 | | 122.45 | | |
| 5 | In | 122.29 | 0.28 | 122.52 | 0.26 | 0.02 |
| | Ex | 122.01 | | 122.26 | | |
| 6 | In | 122.01 | 0.30 | 122.26 | 0.29 | 0.01 |
| | Ex | 121.71 | | 121.97 | | |
| 7 | In | 121.71 | 0.29 | 121.97 | 0.29 | 0.00 |
| | Ex | 121.42 | | 121.67 | | |
| | | 121.42 kPa | 2.07 kPa | 121.67 kPa | 1.8 kPa | |

The change in air speed at the section, vertical to the hose that was taken from the region where geometric deformation is maximum according to the analysis results, is given in Fig. 17.

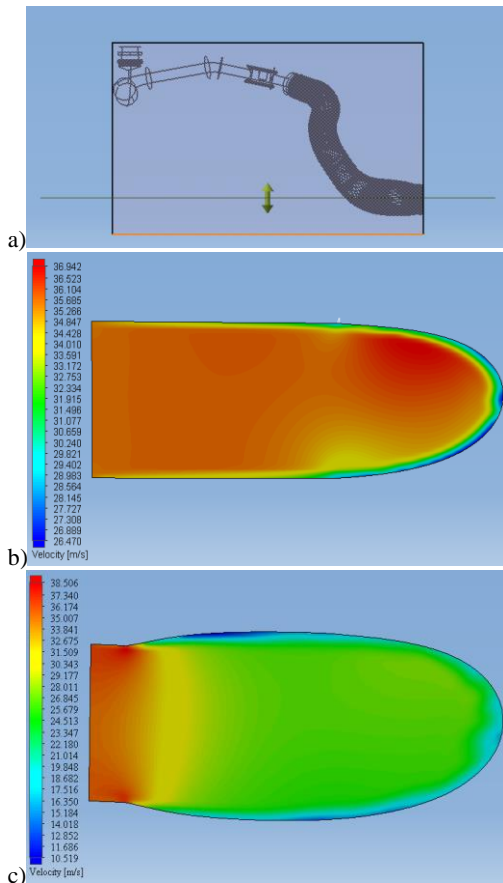


Fig. 17. Speed distribution a) Section b) Undeformed air pipe c) Deformed air pipe in maximum deformation section.

The results of pressure distribution at the section indicated in Fig. 17 a is given in Fig. 18.

The change in the temperature throughout the hose is

given in Fig. 17. The air that entered the hose at $T_{in}=100^{\circ}C$ was determined to exit at $T_{out}=99.29^{\circ}C$ for deformed hose and $T_{out}=99.44$ undeformed hose. The value of change in temperature was calculated as $\Delta T= 0.71-0,6^{\circ}C$.

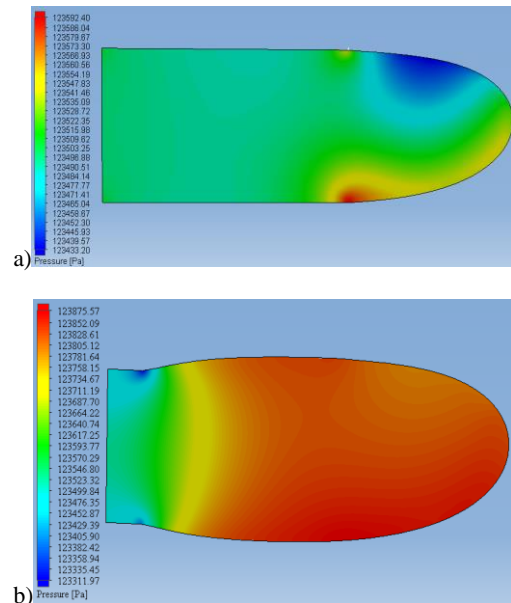


Fig. 18. Total pressure distribution a) Undeformed b) Deformed air pipe in maximum deformation section.

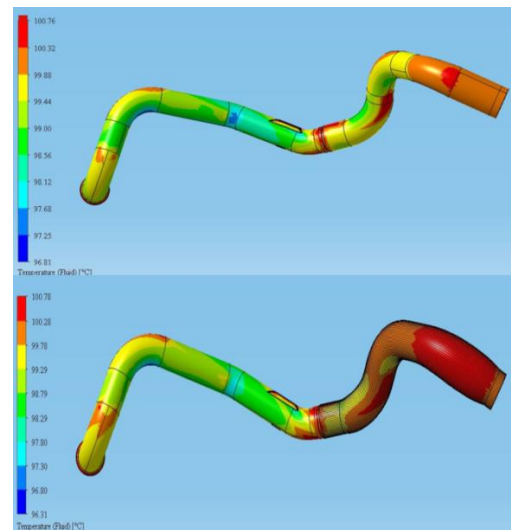


Fig. 19. Temperature distribution.

4. DISCUSSION

According to the analysis results, the total pressure losses for deformed and undeformed hose geometries were determined as $\Delta P_K= 2.04$ kPa, 1.85 kPa, respectively. As is seen from Fig. 15 a and b, the inlet pressures in the hose were determined above 123.5 kPa. The reason of that can be explained with the fact that pressure and speed values at momentum transfer mechanism change due to bends and geometric differentiations in the hose. The pressure values also change due to the change in air speed in terms of both direction and size during the flow.

When the pressure loss values were evaluated according to the analysis results, pressure loss at both two geometries, for deformed and undeformed geometry, were determined as 1.2 kPa, 1.04 kPa respectively. The comparison of these values with total pressure loss value are given in Table 6. It was determined that 56% of the total pressure loss took place at deformed geometry, 54% took place at undeformed geometry (at rubber hose). It was also found that the pressure loss at PA6 GF 30 hose part was nearly the same, a small difference of 0.03 kPa occurred.

Table 8 Pressure lose according to material

| | Total ΔP_k | Rubber Part ΔP_k | PA Part ΔP_k |
|-----------------------|--------------------|--------------------------|----------------------|
| Deformed | 1.85 kPa | 1.04 kPa | 0.81 kPa |
| Undeformed | 2.04 kPa | 1.2 kPa | 0.84 kPa |
| Difference ΔP | 0.19 kPa | 0.16 kPa | 0.03 kPa |

When the rubber hose where more than 50% of the pressure loss took place was examined, it was seen that the geometric deformation positively affected the pressure loss, and caused less pressure loss. But, the decrease in flow rate and accordingly increase in pressure loss with the increase in hose inner diameter is supposed to happen at deformed geometry. When Fig. 17 b and c compared, it was seen that maximum air speed at the section (Fig. 17 a) gotten from the deformed region was reached at the deformed geometry. Although maximum speed value was reached, the average speed value at the deformed geometry was found to reach 24 m/s. In spite of that, the air speed at the undeformed hose was found higher (31 m/s) than that at more homogenous and average one.

As well as the decrease in speed is supposed to decrease the pressure, the pressure loss at deformed geometry was found not so much depending on the deformation-associated highness of the speed and momentum change. As is seen in Fig. 18 a and b, the average total pressure on the inlet section where the decrease in the average speed didn't affect the pressure loss so much was calculated as 123.520 kPa at deformed geometry, 123.440 kPa at undeformed geometry. In the light of these data, the diameter enlargement-oriented deformation that occurred because of the pressure forces was found to have not much negative effect on the pressure loss. In the study, the pressure distribution graphics on the curve passing from the center of the deformed and undeformed hose geometry are given in Fig. 20. As is seen from Fig. 20, there is no any similarity at pressure distribution curves belonging to the deformed rubber hose part. According to the calculated values, less pressure loss occurred at deformed geometry part.

As can be seen in Fig. 20, pressure distribution profile at PA6 GF15 part was determined as similar and differ by very small pressure difference. As is seen in Table 6, there is a pressure loss of 0.03 kPa at PA6 GF15 hose part.

In the study, less pressure loss was found at the

deformed hose. A research was performed on if the reason of that could be the bends that can cause pressure losses, which is suggested by Table 5 data. It was determined that the sharp bends transformed into wider-angle bends at the rubber hose part, the geometry of which changed with pressure forces (Fig. 21). It was thought that the pressure gain of 0.16 kPa (Table 6) at the rubber hose which underwent a geometric deformation was due to the differentiation of the bends at the flow geometry.

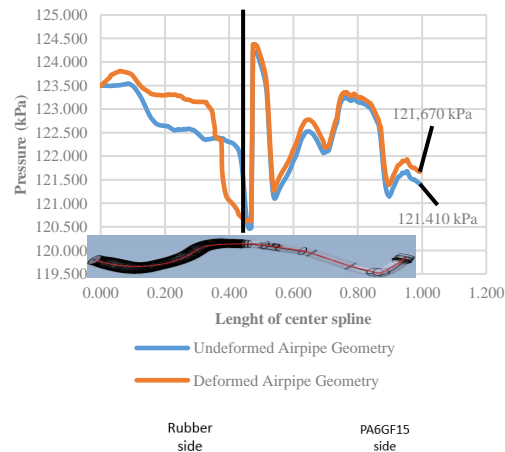


Fig. 20. Pressure distribution on center spline of air pipe.

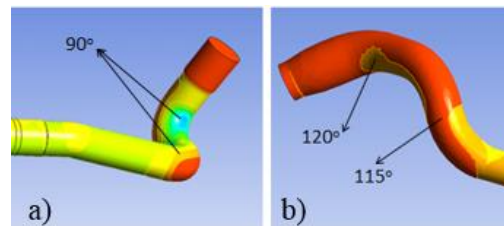


Fig. 21. Rubber part a) Undeformed hose b) Deformed hose.

In this study, the pressure loss at rubber hose part was determined as 1.04 kPa and 1.2 kPa respectively at the deformed and undeformed geometry. In the study by Uysal *et al.* (2012) the pressure loss at the rubber hose was determined as 0.93 kPa. In both study, the surface roughness ratio of rubber material was assumed as 0.32 μm . While the length of the rubber hose included in our study is 410.8 mm, that included in the study by Uysal *et al.* (2012) is 428.9 mm. The deformation that would likely occur on the rubber hose- included in the study by Uysal *et al.* (2012) - by pressure forces was neglected. Not taking deformation into account and an excessiveness of 18.1 mm at the length of the hose might be effective in the occurrence of the pressure loss of 0.93 kPa in the study by Uysal *et al.* (2012)

When compared with the study by Uysal *et al.* (2012) total pressure loss was seen to be maximum in this study. That can be due to the reasons such as the air hose used in the study by Uysal *et al.* (2012) consists of metal and rubber materials; the hose length in that study is longer than that in this study; the metal roughness ratio (0.32 μm) used in that study is lower

than PA6 GF30 hose surface roughness ratio (1.85 μm) used in this study. The surface roughness ratio assumed for PA6 GF30 hose in this study (Satheeskumar and Kanagaraj 2016). As a result of the comparison of the pressure loss at metal tube and PA6 GF15 hose, a pressure loss of 0.7 kPa was determined at metal tube, and that of 0.84 kPa at undeformed geometry of GF15 hose. The reason why the pressure loss yielded high in this study is thought due to the fact that the length of the hose made of PA6 GF15 material used in this study is 143 mm longer, and that its surface roughness ratio is higher than metal material's.

Since their air flow rates, especially deformation, and hose lengths were different, air velocities showed difference. This difference already was reflected to the pressure values. In the study by Uysal *et al.* (2012) the maximum air speed, 50 m/s, was seen at the sharp bend sections. In this study, while maximum air speed realized as 70 m/s at undeformed geometry, it reached up to 74 m/s at deformed geometry.

The change in temperature throughout the hose in this study was $\Delta T = 0.71\text{--}0.6^\circ\text{C}$ for both geometry, whereas it was found to be a near value at $\Delta T = 0.8^\circ\text{C}$ in the study conducted by Uysal *et al.* (2012) (Fig. 18 c, Fig. 17).

5. CONCLUSION

Our study has revealed based on the analysis results that the deformation amount that vehicle hoses made of rubber material undergo due to pressure forces should be considered at air hose pressure loss analyses where that deformation acted in the direction of reducing pressure loss. It is recommended that the geometric deformation of the rubber hose is taken into consideration in the calculation of the pressure loss in the air hoses. It has been determined that elastic behavior of rubber material directly affects pressure loss. The utilization of FSI method is recommended especially to define the deformation of rubber material at the critical values of pressure loss. The literature shows that materials used in air hoses affect pressure loss depending on surface roughness value. The importance of CFD application in the determination of pressure loss value at air hoses have been confirmed by this study. The use of FSI method, especially in the determination of the deformation at the geometry, occurring with the effect of pressure forces, helps in obtaining real-like results. In addition to the effects of geometric deformation on pressure loss, the effect of vibration in the z direction hose on pressure loss can be investigated by researchers in acceleration tests.

REFERENCES

- Abdullah, N. R., N. S. Shahrudin, A. M. I. Mamat, S. Kasolang, A. Zulkifli and R. Mamat (2013). Effects of air intake pressure to the fuel economy and exhaust emissions on a small SI engine. *Procedia Engineering* 68, 278–284.
- Baaser, H. (2007). Global optimization of length and macro-micro transition of fabric-reinforced elastomers with application to a brake hose. *Computational Materials Science* 39(1 SPEC. ISS.), 113–116.
- Bhakade, S., T. Ashta and S. Patil (2016). Deformation Analysis of Flexible Hose used in Air Intake System of Automobile using CFD and FEA, *International Conference on Design, Manufacturing and Mechatronics*, At Trinity College, Pune.
- Chaubey, A. and P. A. C. Tiwari (2017). Design and CFD Analysis of The Intake Manifold for the Suzuki G13bb Engine5(Vi), 1258–1276.
- Choi, H. and I. Oh, (2010). Analysis of product efficiency of hybrid vehicles and promotion policies. *Energy Policy* 38(5), 2262–2271.
- Gohel, N. S. (2015). CFD Analysis of Air Intake System 4(2), 45–48.
- Gu, S. (2017). Application of finite element method in mechanical design of automotive parts. *IOF Conference Series: Materials Science and Engineering*, 231(1), 012180.
- Kamarulbaharin, Z. A. and S. Kasolang (2015). Flow behaviour analysis along an engine air intake pipe. *Jurnal Teknologi*, 76(10), 65–69.
- Kumar, J. S. and V. Ganesan (2004). Flow through S.I. engine air intake system using CFD at part throttle and full throttle. *Indian Journal of Engineering and Materials Sciences* 11(2), 93–99.
- Kumar, N. and V. V. Rao (2016). Hyperelastic Mooney-Rivlin Model: Determination and Physical Interpretation of Material Constants. *MIT International Journal of Mechanical Engineering* 6(1), 43–46.
- Mamat, R., N. Rosli Abdullah, H. Xu, M. L. Wyszynski, and A. Tsolakis (2017). Effect of air intake pressure drop on performance and emissions of a diesel engine operating with biodiesel and ultra low sulphur diesel (ULSD). *Renewable Energy and Power Quality* 1(07), 787–794.
- Ramasamy, D., M. Zamri, S. Mahendran, and S. Vijayan (2010). Design Optimization of Air Intake System (AIS) of 1.6L Engine by Adding Guide Vane. *The International MultiConference of Engineers and Computer Scientists (IMECS)*, Hong Kong.
- Rao, A. (2003). Fluid-solid interaction analysis using ANSYS/multiphysics. *Computational Fluid and Solid Mechanics 2003*, 1492–1496.
- Safwan, M. and B. A. Lothfy (2009). *Pressure Drop analysis of 1.6 L car Air intake system*, Doctoral dissertation, UMP.
- Satheeskumar, S. and G. Kanagaraj (2016). Experimental investigation on tribological behaviours of PA6, PA6-reinforced Al₂O₃ and PA6-reinforced graphite polymer composites.

- Bulletin of Materials Science* 39(6), 1467–1481.
- Sedlacek, F. and M. Skovajsa (2016). Optimization of an Intake System Using CFD Numerical Simulation. *Proceedings in Manufacturing Systems* 11(2), 71–76.
- Uysal, A., M. Ozalp, A. Korgavus, and O. Korgavus (2012). Numerical modeling of the momentum and thermal characteristics of air flow in the intercooler connection hose. In *International Journal of Advanced Manufacturing Technology* 60, 811–824.
- Williams, C. B. and R. Ilardo(2010). Design and manufacture of a Formula SAE intake system using fused deposition modeling and fiber-reinforced composite materials. *Rapid Prototyping Journal* 16(3), 174–179.
- Yerram, R., Prasad, N., Malathkar, P. R., Halbe, V., & Murthy, S. D. (2006). Optimization of Intake System and Filter of an Automobile using CFD analysis. *Quality Engineering & Software Technologies* (QUEST), Bangalore, India.